Title
Texture and elastic anisotropy of a mylonitic anorthosite from the Morin Shear Zone (Quebec, Canada)

Authors
Barreiro, Juan Gómez
Wenk, Hans-Rudolf
Vogel, Sven

Publication Date
2015-02-01

DOI
10.1016/j.jsg.2014.07.021

Peer reviewed

Journal of Structural Geology 71 (2015) 100–111

Contents lists available at ScienceDirect

Journal of Structural Geology

journal homepage: www.elsevier.com/locate/jsg

Texture and elastic anisotropy of a mylonitic anorthosite from the Morin Shear Zone (Quebec, Canada)

Juan Gómez Barreiro [a, *], Hans-Rudolf Wenk [b], Sven Vogel [c]

[a] Departamento de Geología, Universidad de Salamanca, Pza. de los Caídos s/n, 37008 Salamanca, Spain
[b] Department of Earth and Planetary Science, University of California, Berkeley, CA 94720, USA
[c] Los Alamos Neutron Science Center, Los Alamos National Laboratory, NM 87545, USA

ARTICLE INFO

Article history:
Available online 19 August 2014

Keywords:
Pyroxene plagioclase texture
Neutron diffraction
Anorthosite
Elastic properties
Seismic anisotropy
Grenville province

ABSTRACT

A sample of anorthosite from the granulite facies Morin Shear Zone (Quebec, Canada) was investigated for crystal preferred orientation and elastic anisotropy. Time-of-flight neutron diffraction data obtained with the HIPPO diffractometer at LANSCE were analyzed with the Rietveld method to obtain orientation distribution functions of the principal phases (plagioclase, clinopyroxene and orthopyroxene). Texture and microstructures are compatible with the plastic deformation of the aggregate under high-T conditions. All mineral phases depict a significant preferred orientation that could be related to the general top-to-the north shearing history of the Morin Shear Zone. Texture patterns suggest that (010)[001] in plagioclase and (110)[001] in clinopyroxene are likely dominant slip systems. Using preferred orientation data P- and S-waves velocities and elastic anisotropy were calculated and compared with previous studies to explore elastic properties of rocks with different pyroxene-plagioclase mixtures. P-wave velocity, S-wave splitting and anisotropy increase with clinopyroxene content. Seismic anisotropy is linked to the texture symmetry which can lead to large deviations between actual anisotropy and that measured along Cartesian *XYZ* sample directions (lineation/foliation reference frame). This is significant for the prediction and interpretation of seismic data, particularly for monoclinic or triclinic texture symmetries.

1. Introduction

It has been proposed that the deformation of continental lithosphere is mainly driven by the mechanical response of the lower crust (e.g. Royden et al., 1997; Ranalli, 1995, 2003; Rutter and Brodie, 1992). Geophysical observations (e.g. Chen and Molnar, 1983; Wong and Chapman, 1990), thermomechanical models (e.g. Beaumont et al., 2001) and extrapolation of experimental flow laws (e.g. Brace and Kohlstedt, 1980; Kohlstedt et al., 1995; Dimanov et al., 2007) point to a model of long-term strength for the lithosphere with a relatively weak lower crust, placed between a stronger upper crust and mantle (Burov and Watts, 2006). Thermal and compositional heterogeneity of the lithosphere result in a variety of rheological behaviors across tectonic plates and alternative models could play a significant role in some geodynamic contexts (e.g. Maggi et al., 2000; Jackson, 2002). Those features evolve with time and one should consider rheological boundaries as dynamic entities in the Earth system (e.g. Bürgmann and Dresen, 2008).

High-strain zones are recognized as essential pieces of that architecture, but the proportion of localized to distributed strain-flow with depth is not well understood (Ellis and Stöckhert, 2004; Bürgmann and Dresen, 2008). The existence of a laminated lower crust, as revealed by seismic surveys, could be interpreted as the result of localized strain, supporting the role of shear zones (e.g. Franke, 1995; Rey, 1995; Cook et al., 1997; Ji et al., 1997). It is clear that interpretations of seismic data, both in structural and lithological terms, has to rely on a quantitative knowledge of the mechanical properties of shear zones.

Most rock-forming minerals are elastically anisotropic. When deformed in a high-strain zone, crystal preferred orientation or texture often develops. Therefore the aggregate of minerals in deformed rocks will show macroscopic anisotropy (e.g. Kocks et al., 2000), and potentially become a highly reflective volume in the lithosphere (e.g. Ji et al., 1997).

The dominant mineral phases in the lower crust are plagioclase and pyroxene (e.g. Tullis, 1990; Ji et al., 2004a,b; Dimanov et al., 2007). Both exhibit strong anisotropy of their physical properties

* Corresponding author. Tel.: +34 923294488; fax: +34 923 29 4514.
E-mail addresses: jugb@usal.es (J. Gómez Barreiro), wenk@berkeley.edu (H.-R. Wenk), sven@lanl.gov (S. Vogel).

http://dx.doi.org/10.1016/j.jsg.2014.07.021
0191-8141/

as single crystals (e.g. Brown et al., 2006; Jackson et al., 2007; Sang et al., 2011; Kaercher et al., 2014), and a contrasting mechanical behavior, with plagioclase as the weak phase (e.g. Mackwell et al., 1998; Dimanov and Dresen, 2005).

Exploring the crystallographic preferred orientation of deformed pyroxene-plagioclase aggregates could lead to a better understanding of the mechanical and seismic properties of lower crust shear zones. Previous work has focused on texture development of plagioclase aggregates, both naturally and experimentally deformed (e.g. Ji and Mainpraice, 1988; Ji et al., 1997; Rybacki and Dresen, 2000; Xie et al., 2003; Feinberg et al., 2006; Gómez Barreiro et al., 2007; Homburg et al., 2010). By comparison, relatively little is known about texture in metabasites (e.g. Mehl and Hirth, 2008; Kanagawa et al., 2008; Gómez Barreiro et al., 2010; Gómez Barreiro and Martínez Catalán, 2012). Moreover, our knowledge of deformation mechanisms of plagioclase and pyroxene are incomplete (e.g. Dornbusch et al., 1994; Bascou et al., 2002; Gómez Barreiro et al., 2007).

In previous studies mylonites from an anorthositic shear zone in Canada (Morin Shear Zone) have been analyzed. Only the texture of plagioclase was investigated in some detail (e.g. Ji et al., 1994, 1997; Zhao, 1997; Xie et al., 2003). Since then texture analysis evolved from the limited and time consuming U-stage procedures and pole figure goniometry to electron backscatter diffraction (EBSD), synchrotron X-ray diffraction and neutron diffraction. Here we are revisiting this natural laboratory to apply time-of-flight (TOF) neutron diffraction and advanced data analysis to quantify the texture of not only plagioclase but also pyroxene (e.g. Gómez Barreiro and Martínez Catalán, 2012). Based on preferred orientation patterns we then model elastic properties of anorthosite mylonite and finally extend the results to explore elastic anisotropy of rocks with different plagioclase-pyroxene contents to discuss the compositional effect on the physical properties of mafic mylonites (Lloyd et al., 2011).

2. Geological context

The Morin Terrane is part of the Allochthonous Monocyclic Belt, in the SE of the Grenville Province, Canada (Rivers et al., 1989). The Morin Terrane is composed of a Mid-Proterozoic anorthosite suite, surrounded by charnokites, granulites and metasediments (Doig, 1991). For a discussion of the tectonic setting and tectonothermal evolution of the Morin Terrane see Martignole and Friedman (1998), Wodicka et al. (2000) and McLelland et al. (2010).

The Morin anorthosite suite is bounded on the east, by the 5 km-wide Morin Shear Zone (Zhao et al., 1997), which contains a variety of igneous and metasedimentary lithologies. The mylonitic fabrics are defined by quartz ribbons, and flattened aggregates of plagioclase and pyroxene, with a penetrative subhorizontal N0-160E lineation and a west-dipping foliation (Zhao et al., 1997; Ji et al., 1997). Deformation conditions reached granulite facies (630–750 °C/550–750 MPa; Indares and Martignole, 1990). Kinematic criteria at different scales indicate a top-to-the north sense of shear (e.g. Zhao et al., 1997).

3. Sample description

A sample was collected 10 km NW the town of Rawdon (Quebec, Canada) in a mylonitic–ultramylonitic band of meta-igneous rocks. The composition is between a leuconorite and anorthosite, with about 90% plagioclase, 7% clinopyroxene and 3% orthopyroxene. The lineation is defined by elongated pyroxene aggregates and some

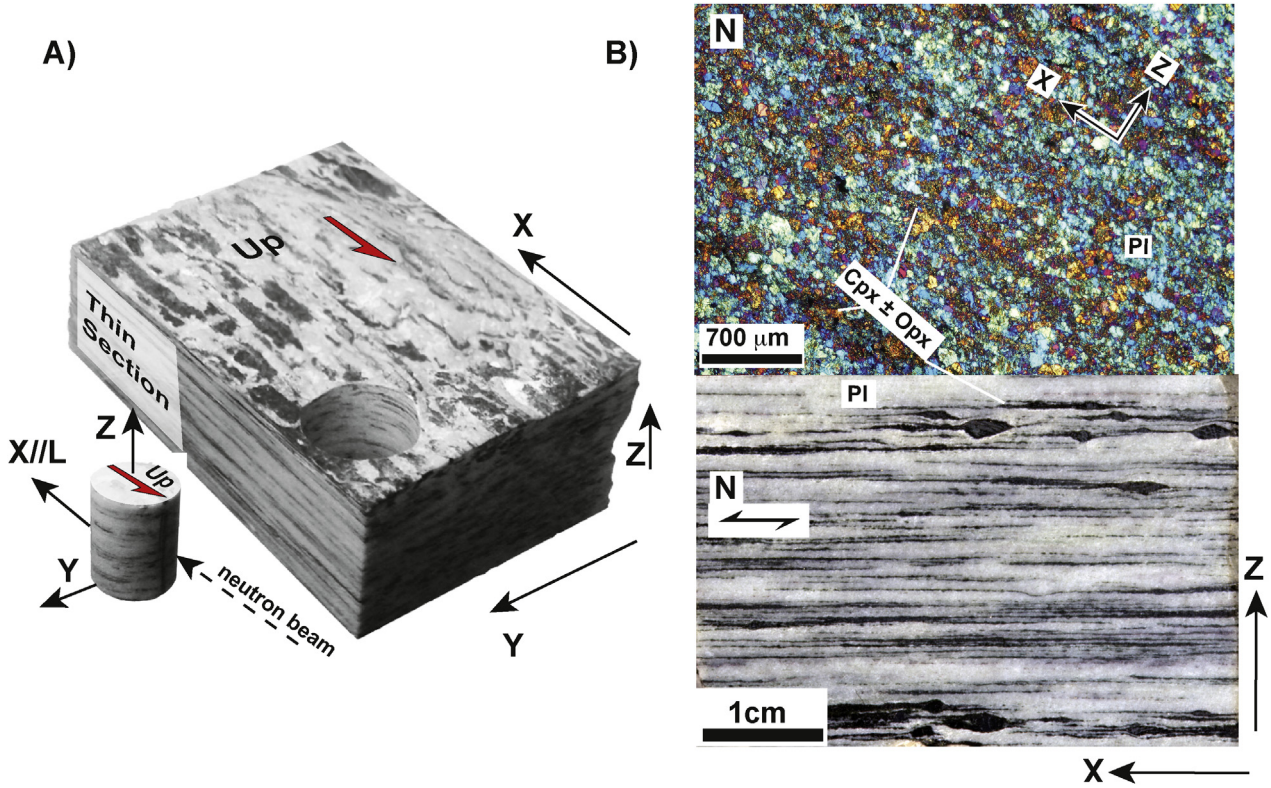

Fig. 1. A) Sample reference system. *X* parallel to the Lineation and foliation define the *XY* plane. The cylinder for TOF neutron diffraction was coring perpendicular to the foliation and with an arrow parallel to *X*-axis. B) Thin section (gypsum plate inserted) to show microstructure and qualitative alignment of plagioclase (blue). Note that the plagioclase crystallographic preferred orientation is heterogeneous. A detail of the mylonitic fabric (*XZ* section) is presented, with fine bands made up of pyroxene. Some asymmetric aggregates of pyroxene indicate a top-to-the North sense of shear. (For interpretation of the references to color in this figure legend, the reader is referred to the web version of this article.)

porphyroclasts give the sense of shearing to the north (Fig. 1A). Pervasive recrystallization is recognized in thin sections (Fig. 1B). Also a view with polarized light and a gypsum plate inserted demonstrates strong crystal alignment (uniform blue color). Plagioclase is fine-grained, with an estimated average grain-size of $d = 50$ μm and a shape ratio (SR = long/short dimension) of 1.5. Some plagioclase ribbons ($d \approx 400$ μm, SR ≈ 6) are locally preserved. Evidence of intracrystalline deformation like undulatory extinction, deformation twins and subgrains are abundant in plagioclase. Pyroxene is concentrated along fine bands with grains that range between 1 mm and 200 μm. Similar microstructures have been described by Ji et al. (1994, 1997), Zhao (1997) and Xie et al. (2003).

4. Neutron diffraction texture analysis

Texture analysis by neutron diffraction is the preferred technique for coarse-grained rocks (e.g. Ullemeyer et al., 1998; Wenk et al., 2010). Due to low absorption of neutrons for most elements, neutrons can easily penetrate large volumes, which results in better grain statistics than surface analysis such as thin sections, X-ray pole figure goniometry, and EBSD (e.g. Gómez Barreiro et al., 2010). The experiment was performed at the Los Alamos Neutron Science Center (LANSCE) with the HIPPO TOF neutron diffractometer (Wenk et al., 2003). HIPPO has excellent counting statistics, which is critical for quantitative texture determinations of rocks. The HIPPO diffractometer has 720-^{3}He-detector tubes, distributed over 30 panels arranged on three banks at different diffraction angles (150°, 90° and 40° 2θ). The different banks have different resolution. The pole figure coverage relative to the incident neutron beam is shown in Fig. 2A.

Oriented cylindrical samples of 10 mm in length and 8 mm in diameter, were drilled perpendicular to the foliation (Z). The lineation (X) is marked and the sample coordinate system X, Y and Z is used as reference to define crystal preferred orientation (Fig. 1A). The sample was rotated around the cylinder axis (perpendicular to the incident neutron beam) into four positions (0°, 45°, 67.5°, 90°) to improve pole figures angular coverage (Fig. 2B). At each position, data were collected for 30 min, resulting in a total exposure time of 120 min. TOF diffraction spectra were analyzed with the Rietveld method as implemented in the software MAUD (Material Analysis Using Diffraction; Lutterotti et al., 1997; Wenk et al., 2010). It provides information about phase proportions and preferred orientation. For texture extraction we were using the E-WIMV algorithm. The orientation distribution function (ODF) cell size was 15°. Crystallographic structures are required in the Rietveld refinement and were loaded in 'cif' format. For monocline phases, the first setting has to be used, in both MAUD and BEARTEX, which requires some transformations (Matthies and Wenk, 2009). For plagioclase we use the structure of andesine (P-1; Fitz Gerald et al., 1986), for clinopyroxene diopside (C2/c1; Tribaudino et al., 2005), and for orthopyroxene enstatite (Pbca; Gatta et al., 2007). Lattice parameters were refined. The ODF was exported from MAUD and then used in BEARTEX to calculate and plot pole figures (Wenk et al., 1998). In this article we use labels for second monoclinic setting for labels in pole figures (i.e., [010] is the 2-fold axis).

It should be noted that due to the low crystal symmetry of major components, for example, clinopyroxene (monoclinic) and plagioclase (triclinic), [100] [010] and [001] directions do not correspond to the pole of the respective crystallographic plane (100) (010) (001), except for [010] in the monoclinic system. To approximate [100] [010] and [001] directions, poles of (20-1) (010) and (−102)

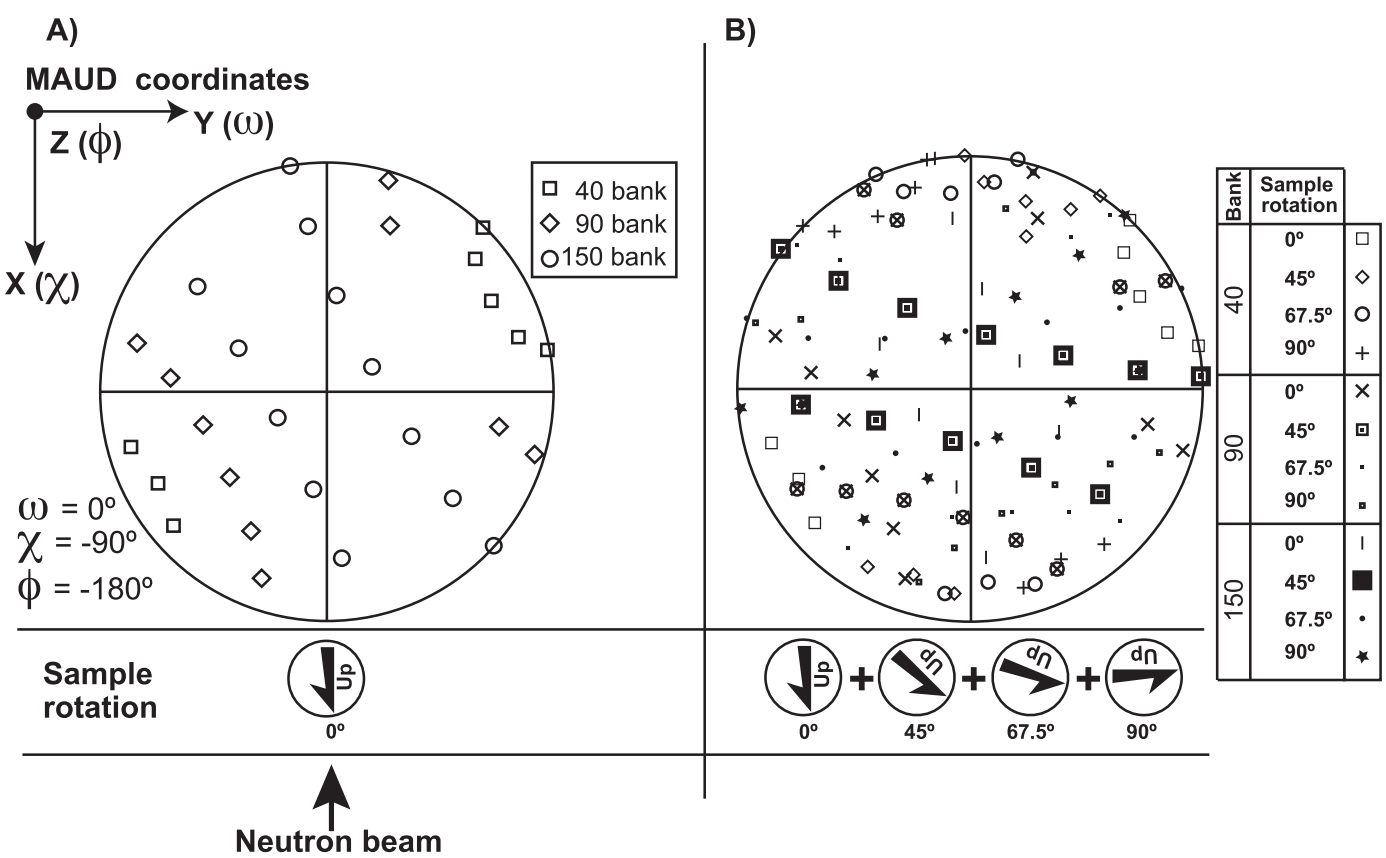

Fig. 2. Pole figure coverage. A) Single rotation. B) Combined sample rotations to improve coverage (0°, 45°, 67.5°, 90°). MAUD coordinates system is indicated with three orthogonal axes and corresponding rotations, χ, ω, φ. System has been rotated around $\chi = -90°$ and $\varphi = -180°$ to bring HIPPO rotation axis to the center of the pole figure and the arrow on top of the sample pointing to the neutron beam at 6 o'clock (Conventional setting). Coverage is plotted relative to sample coordinates.

were used for plagioclase and (−601) (010) (−205) for clinopyroxene (Gómez Barreiro et al., 2007).

Some experimental and calculated diffraction spectra are shown in Fig. 3. Because of the low symmetry of the minerals there is a large number of diffraction peaks, indicated at the bottom, with extreme peak overlaps. Variation of relative intensities of spectra parallel and perpendicular to the foliation is indicative of texture. This is even more evident in the map plot (Fig. 4) which shows a stack of experimental (bottom) and Rietveld model (top) diffraction spectra. The good agreement between experiment and model suggests that the Rietveld fit is reliable.

5. Elastic properties calculations

The elastic properties of the mylonite have been calculated based on averages of single crystal properties over the ODF of each mineral phase, using BEARTEX. Simple averaging schemes, assuming constant stress or strain, provide estimates of the upper and lower bound (Reuss and Voigt averages respectively). Calculation of arithmetic (Hill, 1952) or geometric means (Matthies and Humbert, 1995) is intermediate. These averaging procedures do not consider the influence of grain size, shape, and distribution of phases (microstructure) and particularly the effect that porosity has on the elasticity of rocks. For this, self-consistent and finite element methods have been applied for shales with extreme shape anisotropy and significant porosity (e.g. Vasin, 2013), but for a sample like anorthosite this was not necessary.

As part of the averaging procedure, single crystal elastic constants are required. For intermediate plagioclase elastic constants of triclinic andesine based on *ab initio* simulations (Kaercher et al., 2014) were used. For pyroxene we use diopside elastic constants from Sang et al. (2011), and for orthoenstatite experimental data by Jackson et al. (2007). Single crystal stiffness coefficients are listed in Table 1A.

After calculating the contribution of each mineral phase to the intrinsic elastic properties, the different phases were combined, taking the relative volume fractions into account. Finally hypothetical cases for rocks with different plagioclase–pyroxene compositions were explored.

6. Results

6.1. Volume fraction

Volume fractions for each mineral phase have been obtained with the Rietveld refinement. The best fit was obtained with 88% of andesine, 8% of diopside and 4% of enstatite. These fractions will be used for the calculation of the elastic properties in Section 6.3.

6.2. Texture

The plagioclase in the analyzed mylonite shows moderate crystallographic preferred orientation with a maximum of 2.9 m.r.d. (multiples of a random distribution, 2.89/0.22 m.r.d.;

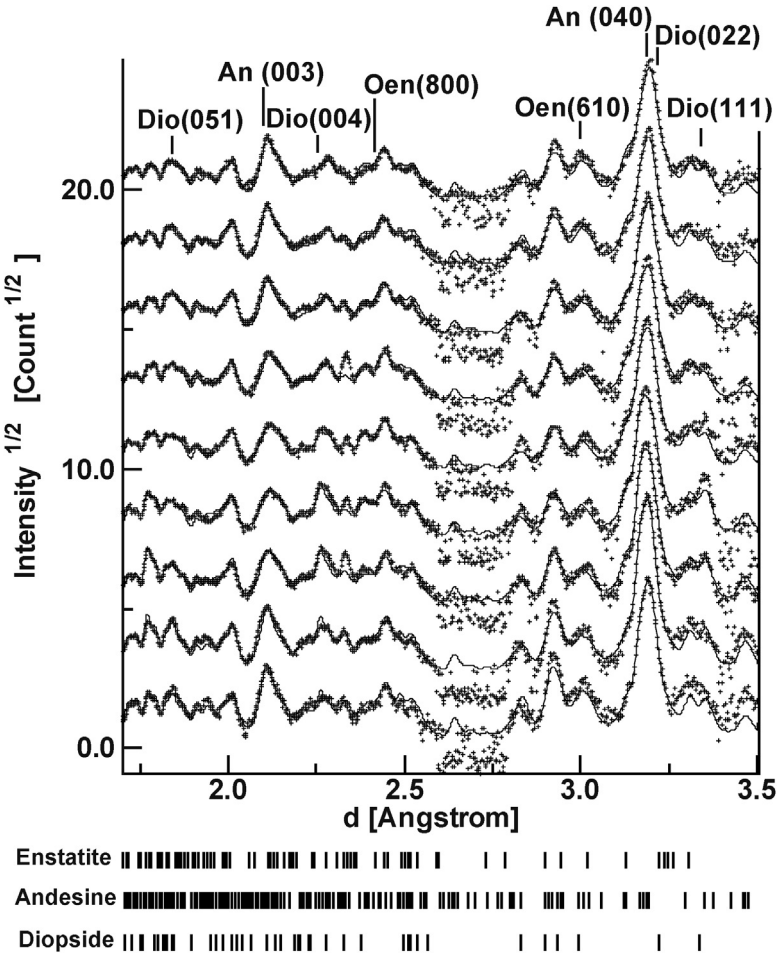

Fig. 3. Selected time-of-flight neutron diffraction spectra, for different angles from the 90 bank. The variation on peak intensity is due to texture. Note the strong peak overlapping at lower d-spacing. The positions of some crystallographic planes are indicated. Crosses are measured data, the lines are the Rietveld fit.

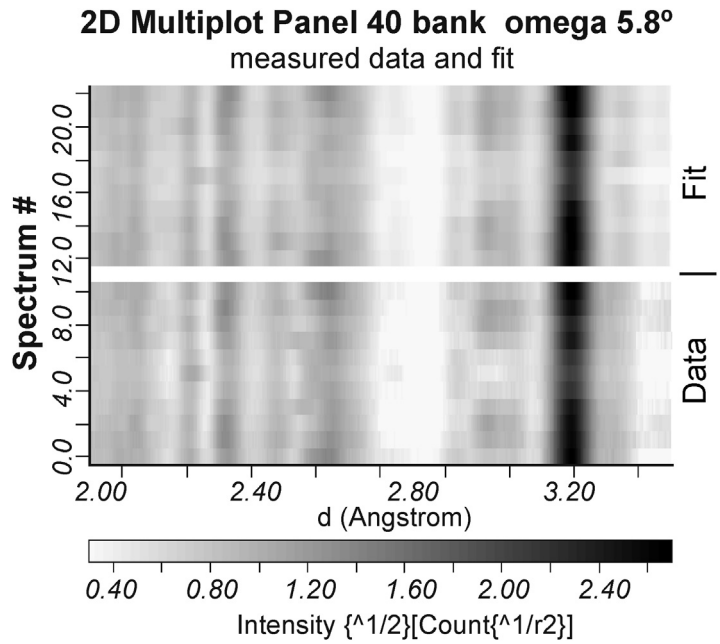

Fig. 4. Multiplot of the 40° bank spectra at rotation angle $\omega = 5.8$. Experimental data below and model (fit) above, after Rietveld refinement. The good agreement suggests that the Rietveld model is reliable.

Fig. 5). The (010) plane defines an asymmetric maximum close to the foliation pole (*Z*-axis). The [001] direction displays a principal maximum close to the lineation of the sample. The [100] axes do not display a clear texture pattern (Fig. 5).

The clinopyroxene texture is strong, with a maximum of about 10 m.r.d. and a very low minimum (0.03 m.r.d.). The (010) planes are parallel to the mylonitic foliation, depicting an orthorhombic fabric symmetry (Fig. 5). The poles of the (110) planes define a slightly

Table 1
A) Single crystal elastic stiffness coefficients. All coefficients are in standard setting ($Z' = c, Y' = (a \times c), X' = (Y' \times Z')$, where X', Y', Z' and a, b, c, are crystal axes. B) Elastic stiffness coefficients for Morin mylonitic anorthosite. Tensor coefficients for andesine, diopside and enstatite polycrystals were calculated averaging single crystal elastic data through the ODFs. Voigt (V) and Geometric Mean (GM) means are presented. Elastic coefficients for the polyphasic mylonitic aggregate (Pl-Cpx-Opx) were calculated based on mineral volume fractions obtained after Rietveld refinement and aggregate density (ρ). Voigt and Geometric Means are shown. C) Stiffness coefficients for selected synthetic mixtures were calculated after mylonitic anorthosite polycrystals and densities, with several combinations of volume fractions. Only the Voigt average is depicted. All Values are in GPa.

C_{ij}	A) Single crystals			B) Morin mylonitic anorthosite								C) Synthetic mixtures					
	Andesine	Diopside	Enstatite	Polycrystal						Polyphase		Leucogabbro		Gabbro		Melagabbro	
	Kaercher et al. (2014)	Sang et al. (2011)	Jackson et al. (2007)	Andesine		Diopside		Enstatite		88 Pl 8 Cpx 4 Opx		70 Pl 30 Cpx		50 Pl 50 Cpx		30 Pl 70 Cpx	
				V	GM	*V*	GM	*V*	GM	*V*	GM	*V*	GM	*V*	GM	*V*	GM
*C*11	99.2	229	236	124.5	118.4	224.5	199.9	210.8	208.9	134.27	126.22	148.3	142.9	164.2	159.2	180.1	175.5
*C*12	50.3	78	74	46.7	48.3	73.7	67.7	56.9	56.6	48.86	50.13	53.2	54.1	57.6	58.0	62.0	61.9
*C*13	38.5	69.8	57	45.9	46.1	68.5	65.1	56.4	56.0	47.96	47.95	52.0	51.8	56.0	55.6	60.1	59.4
*C*14	9.6	0	0	−0.4	−0.3	0.4	−0.2	−0.1	−0.1	−0.35	−0.33	−0.3	−0.3	−0.3	−0.3	−0.2	−0.2
*C*15	−0.2	9.9	0	−0.1	−0.2	−2.5	0.9	−0.5	−0.6	−0.05	−0.12	0.2	0.2	0.4	0.4	0.7	0.6
*C*16	−1.1	0	0	1.9	1.7	1.1	−0.9	0.2	0.2	1.57	1.60	1.0	0.9	0.5	0.4	−0.1	−0.1
*C*22	169.4	179	173	128.8	122.6	216.9	218.0	218.0	216.8	139.99	131.19	157.5	151.2	176.6	170.3	195.8	189.4
*C*23	22	58	50	47.1	48.8	66.2	73.2	58.5	58.3	49.71	50.95	55.1	56.1	60.4	61.0	65.7	65.9
*C*24	−4.8	0	0	0.0	0.0	0.9	1.0	0.1	0.1	0.12	0.06	0.4	0.3	0.6	0.5	0.8	0.7
*C*25	−2.1	6.1	0	−0.1	−0.1	−0.4	0.4	−0.3	−0.3	−0.03	−0.04	0.1	0.1	0.2	0.2	0.2	0.3
*C*26	−2.5	0	0	−0.5	−0.2	0.3	−2.6	0.0	0.0	−0.69	−0.34	−1.1	−0.9	−1.5	−1.4	−1.9	−1.9
*C*33	165.2	242.5	216	123.1	117.2	204.0	211.2	214.5	213.0	134.25	125.72	151.2	145.4	170.0	164.2	188.8	183.0
*C*34	8.7	0	0	−0.2	−0.3	1.0	0.2	0.4	0.6	−0.17	−0.22	−0.1	−0.1	0.0	0.0	0.1	0.1
*C*35	6.7	40.9	0	−0.1	−0.1	−0.9	0.8	−0.5	−0.6	−0.07	−0.06	0.2	0.2	0.4	0.4	0.6	0.6
*C*36	−9.3	0	0	1.1	1.4	−0.2	−0.5	0.7	0.7	0.96	1.34	0.6	0.8	0.3	0.5	0.0	0.1
*C*44	25.1	78.2	84	39.8	35.9	75.2	72.7	78.6	78.0	44.22	39.21	50.5	46.9	57.6	54.3	64.7	61.6
*C*45	−0.5	0	0	0.1	0.0	0.5	−0.9	−0.1	−0.1	0.03	−0.03	−0.2	−0.2	−0.4	−0.4	−0.6	−0.6
*C*46	−0.3	6.6	0	0.1	0.1	−0.9	0.2	−0.1	−0.1	0.10	0.08	0.1	0.1	0.2	0.1	0.2	0.2
*C*55	28.5	68.1	79	39.3	36.1	76.4	73.8	77.6	76.9	43.73	39.37	50.1	47.4	57.3	55.0	64.5	62.5
*C*56	0	0	0	0.0	0.0	0.2	0.5	0.4	0.4	0.05	−0.01	0.1	0.1	0.2	0.2	0.3	0.3
*C*66	37.5	78.2	80	40.7	36.4	75.4	75.0	77.6	77.0	45.03	39.77	51.4	48.0	58.6	55.7	65.7	63.4
ρ g cm^{-3}	2.72	3.26	3.17	2.72		3.26		3.17		2.78		2.89		2.99		3.10	

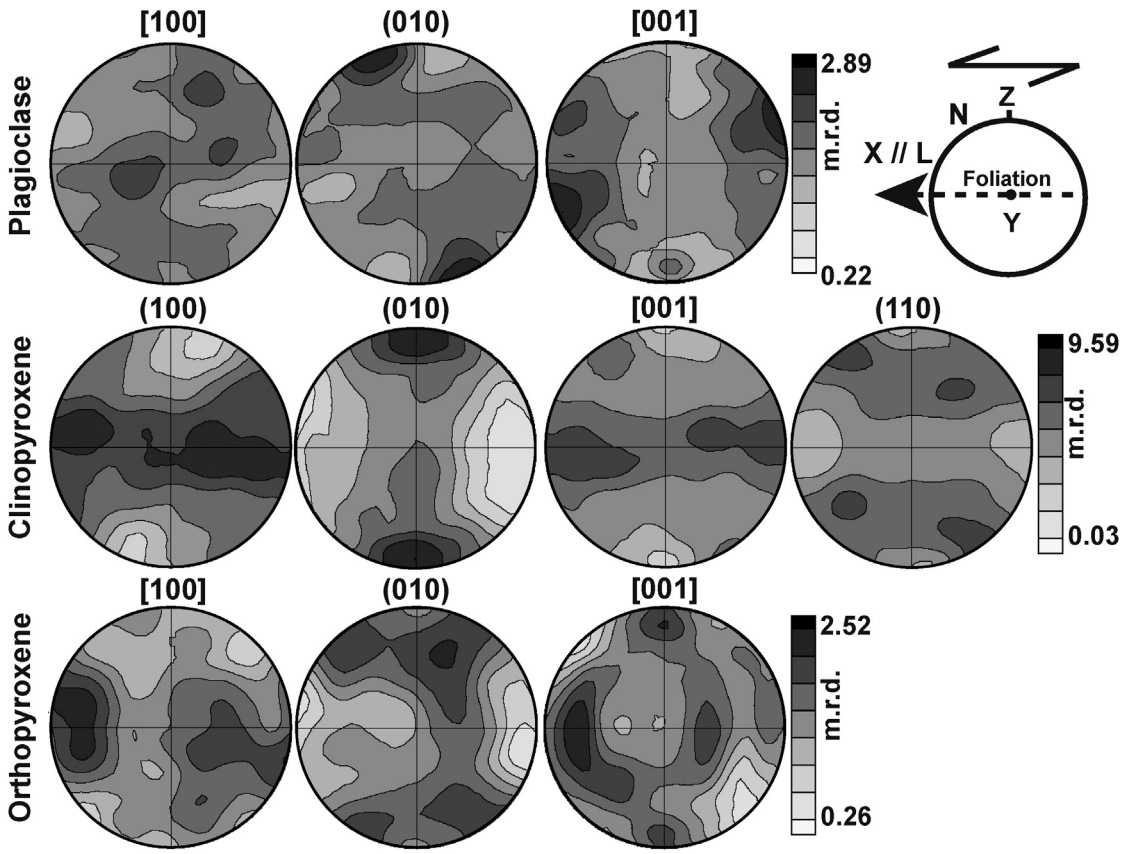

Fig. 5. Pole figures for clinopyroxene (diopside), plagioclase (andesine) and orthopyroxene (enstatite). Reference system is indicated. Contours are in multiples of random distribution (m.r.d.). Equal area projection.

asymmetric small circle around the foliation pole. The [001] axes define an elongated principal maximum close to the lineation (*X*-axis). The poles of (100) planes define an elongated maximum about the foliation.

Orthopyroxene shows a moderate texture, similar in strength to plagioclase (2.52–0.26 m.rd.). Poles of (010) planes define a small circle around the *Z*-axis, and [100] axes are close to the lineation (Fig. 5). The [001] directions define a complex pattern with several maxima. An orthorhombic symmetry dominates the patterns.

6.3. Elastic properties

From the texture of the different phases and their volume fractions the elastic properties of the aggregate can be calculated by averaging. The elastic properties of the single crystal must be taken into account for each mineral phase. In Table 1A [change Kaercher to 2014. Also in the table have a footnote for diopside that this is second setting] single crystal elastic stiffness tensors (C_{ij}) for each mineral phase is shown. For each phase, single crystal elastic tensors (C_{ij}) are averaged over corresponding orientation distributions (ODFs). The results are polycrystal averages for stiffness coefficients of each phase (Polycrystal; Table 1B). Then the polycrystal averages for each phase are combined, taking mineral volume fractions into account. Resultant Polyphase (rock) tensors (C_{ij}) (Polyphase; Table 1B) will be used, with the bulk density (Table 1), to calculate the seismic velocities by the solution of the Christoffel equation.

We used two simple statistical averages in this study: Voigt (V) and Geometric Mean (GM) (Table 1). The Voigt average was selected because it represents an upper bound model, and has been used by several authors for geological systems (e.g. Seront et al., 1992; Ji and Salisbury, 1993; Ji et al., 1997; Zhao, 1997). The Geometric Mean is a robust estimation of the mean value (Matthies and Humbert, 1995). For these calculations and plotting we use programs in the BEARTEX package (Wenk et al., 1998).

In Fig. 6 we show the single crystal propagation surfaces for seismic P-waves (A) and shear-wave splitting (B) for plagioclase, clinopyroxene and orthopyroxene. Standard conventions have to be used for averaging calculations: $Z' = c$, $Y' = (c \times a)$, $X' = (Y' \times Z')$; where X', Y', Z' are axes of the right-handed Cartesian crystal coordinate system and a, b, c are crystal axes (Fig. 6). For monoclinic diopside, the first setting ($Z' = c = [001]$) has been used (Matthies and Wenk, 2009). For shear-wave splitting we also show the orientation of the fast shear wave.

Seismic velocity data for the combined rock are summarized in Table 2. P-wave anisotropy (A; %) is defined as $AV_P = 200^*(V_{Pmax} - V_{Pmin})/(V_{Pmax} + V_{Pmin})$. When the anisotropy is calculated from V_P measurements along *X*, *Y*, *Z* sample axes (Fig. 1), it is calculated as $AV_{P(xz)} = 100^*(V_{Pmax} - V_{Pmin})/V_{Pmean}$, where $V_{Pmean} = (V_{PX} + V_{PY} + V_{PZ})/3$. The two are different when textures are asymmetric. Elastic wave surfaces for P-waves and shear-wave splitting are also displayed in Fig. 7.

The maximum P-wave velocity for the polyphase aggregate is very close to the pole of the mylonitic foliation, and almost parallel to the plagioclase (010) pole maximum (Figs. 5 and 7). As expected, the Voigt average results in higher values than the Geometric Mean. V_P anisotropy, based on actual maximum and minimum, is moderate $AV_P = 2.6–2.4\%$. The anisotropy based on V_P measurements along *X*, *Y*, *Z* sample axes (Fig. 1) (i.e. V_{Px}, V_{Py} and V_{Pz}) is lower ($AV_{P(x-z)} = 2.2–1.9\%$). This effect is due to the asymmetry of the texture. Shear-wave splitting shows a complex distribution, slightly

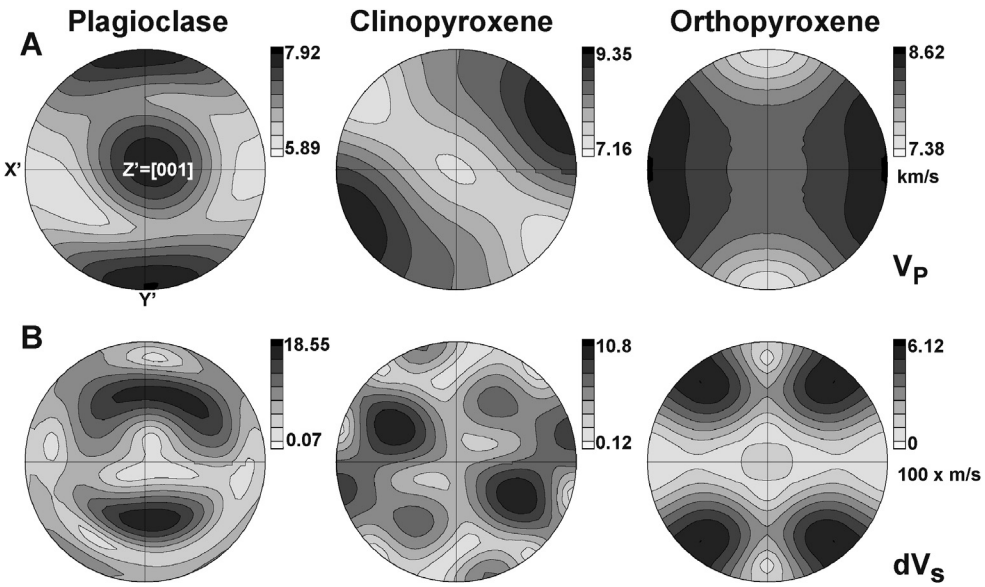

Fig. 6. Single crystal elastic wave propagation surfaces for andesine (An50), diopside, and Enstatite. (A) P-waves and (B) Shear-wave splitting. [001] is in the center (*Z'*) and pole to (010) to the bottom (*Y'*). Equal area projection. Contours are with linear scale. For (B) a velocity difference 10 means 1000 m/s.

dependent on the selected average (Voigt-Geometric Mean; Fig. 7) with four principal maxima. Values are moderate (dVsmax = 97–86 m/s; Table 2). The maximum splitting occurs at about 15° to the lineation and a second one at 15° to the foliation pole, with the first enhanced by Voigt average and the second by the Geometric Mean (Fig. 7). Both the shape of the P and S – wave propagation surfaces correlate well with the plagioclase single crystal and polycrystal patterns (Figs. 5–7).

7. Discussion

7.1. Texture of phases and slip systems

Neutron diffraction analysis of a mylonitic anorthosite from the Morin Shear Zone provides quantitative texture data for plagioclase, clinopyroxene and orthopyroxene (Fig. 5). Previous texture studies on similar rocks from Ji et al. (1994, 1997), Zhao (1997) and Xie et al. (2003) depicted similar patterns for plagioclase. To date very limited information existed for pyroxene (Zhao, 1997) or were assumed to be randomly oriented.

Plagioclase texture patterns are compatible with dislocation activity on (010) planes and [001] directions (Gómez Barreiro et al., 2007, and references therein). A secondary maximum close to the periphery in the [001] pole figure could be related to twining (Fig. 5). The (010)[001] slip system is common in natural plagioclase-rich mylonites at medium to high-grade metamorphic conditions (Kruhl, 1987; Ji et al., 1988, 1994; Zhao, 1997). Dynamic recrystallization is an important process in the Morin Shear Zone and could contribute to the texture (e.g. Ji and Mainprice, 1990; Kruse et al., 2001, 2002). The monoclinic asymmetry of the patterns is coherent with a top-to-the north shearing.

Table 2
Texture based P-waves velocities (V_P), S-wave splitting (dVs), and actual anisotropy (AV_P) from mylonitic anorthosites of the Morin Shear Zone (this study; Xie et al., 2003; Ji et al., 1997; Zhao, 1997). For comparison with ultrasonic measurements (Ji et al., 1997; Zhao, 1997), P-waves velocity was calculated along *X*, *Y* and *Z* sample coordinates (Fig. 1). The P-wave anisotropy ($AV_{P(xz)}$) is shown. Available Voigt (V) and Geometric Mean (GM) averages are presented. The aggregate densities are indicated.

	Morin anorthosite												
	Texture based models								Ultrasonic measurements				
	This study		Xie et al. (2003)	Ji et al. (1997)	Zhao (1997)				Ji et al. (1997)			Zhao (1997)	
%	88 Pl 8 Cpx 4 Opx		95 Pl 5 Px	MT-8 90 Pl 5 Cpx 5 Opx	A1 95 Pl 4 Opx 1 Bt	A2 89 Pl 9 Opx 2 Bt	A4 90 Pl 8 Opx 2 Bt-op	A6 89 Pl 10 Opx 1 Bt	MT-7 85–95 Pl 1–5 Cpx 4–10 Opx	MT-8	MT-9	A4 90 Pl 8 Opx 2 Bt-op	A6 89 Pl 10 Opx 1 Bt
Average	*V*	GM	GM	*V*	*V*	*V*	*V*	*V*					
V_{Pmax} (km/s)	7.10	6.86	6.71	7.00	7.10	7.00	7.03	7.20	–	–	–	–	–
V_{pmin} (km/s)	6.92	6.7	6.49	6.80	6.52	6.71	6.70	6.71	–	–	–	–	–
dVsmax (m/s)	97	86	–	–	300	200	200	400	–	–	–	–	–
dVsmin (m/s)	1	0	–	–	0	0	0	0	–	–	–	–	–
AV_p (%)	2.57	2.36	3.33	2.90	8.50	4.20	4.80	7.00	–	–	–	–	–
V_{PX} (km/s)	6.94	6.73	–	6.92	–	–	–	–	6.75	6.95	6.56	6.57	6.95
V_{PY} (km/s)	6.94	6.71	–	6.80	–	–	–	–	6.67	6.88	6.59	6.60	6.88
V_{PZ} (km/s)	7.09	6.86	–	6.95	–	–	–	–	6.66	6.85	6.48	6.49	6.85
V_p mean	6.99	6.77	–	6.89	–	–	–	–	6.69	6.89	6.54	6.55	6.89
$AV_{p\ (xz)}$ (%)	2.15	1.92	–	2.18	–	–	–	–	1.35	1.45	1.22	1.68	1.45
ρ (g/cm^3)	2.78		–	2.82	–	–	–	–	2.68	2.82	2.68	–	–

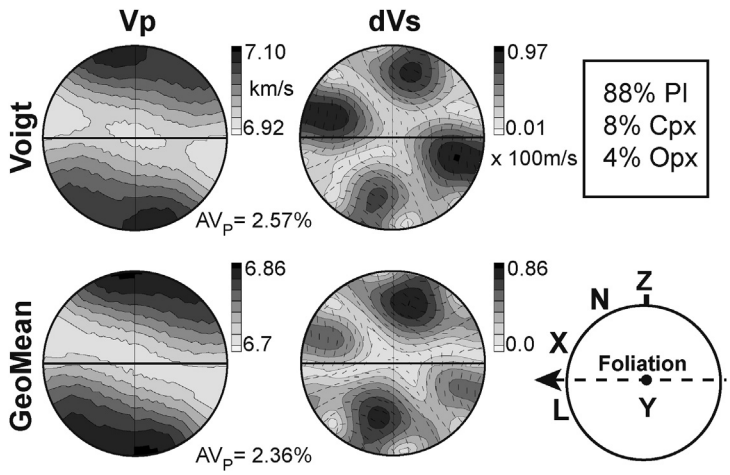

Fig. 7. P-wave velocity (V_P) and S-wave splitting (dVs) propagation surfaces for the mylonitic anorthosite of this study. The results for Voigt and Geometric mean averages are presented. Actual P-wave anisotropy (AV_P, %) is indicated. Equal area projection. Contours are with linear scale.

The crystallographic preferred orientation of clinopyroxene shows a distribution with (010) planes parallel to the foliation and [001] directions parallel to the rock lineation (Fig. 5B). This is a very common texture, both in natural and experimentally deformed clinopyroxene (e.g. Van Roermund and Boland, 1981; Van Roermund, 1983; Buatier et al., 1991; Skrotzki, 1994; Godard and Van Roermund, 1995; Bascou et al., 2001; Brenker et al., 2002). TEM investigations of omphacite (e.g. Godard and Van Roermund, 1995) and diopside (e.g. Amiguet et al., 2010) have not observed dislocation activity on the (010)[001] system. The activation of other slip systems at different temperatures was documented in experiments. Below 800 °C and high stress/strain rate mechanical twinning on planes (100) and (001) dominates (e.g. Avé Lallemant, 1978). At higher temperatures dislocation and diffusion creep control the deformation, depending on microstructure and stresses (e.g. Bystricky and Mackwell, 2001). The systems (100)[001], (010)[100] and {1–10}½<110> have been documented when deformation is carried out at 800–900 °C (Ingrin et al., 1991). At higher temperatures (>1000 °C) {1–10}½<110> and {110}[001] slips dominate (Ingrin et al., 1991; Raterron et al., 1994; Amiguet et al., 2010).

Bascou et al. (2002) attributed the (010)[001] texture in clinopyroxene to a geometrical effect. In a series of Viscoplastic Self Consistent (VPSC) texture simulations on omphacite, those authors demonstrated that even with no slip activity allowed on (010)[001], (010) planes align with the foliation in different strain regimes. Simulation results are compatible with TEM observations and support that slip on {110} controls the orientation of (010) poles normal to the foliation. In our sample, clinopyroxene (110) (010) (100) [001] patterns correlates with simulations of Bascou et al. (2002) and are compatible with a slip on the (110)[001] system.

The dispersion of maxima in the orthopyroxene texture precludes a clear interpretation in terms of slip systems. While (100)[001] and (010) [001] have been suggested as important slip system for high-grade metamorphic conditions (Avé Lallemant, 1978; Ross and Nielsen, 1978; Christensen and Lundquist, 1982; Dornbusch et al., 1994), the contribution of other mechanisms like grain boundary sliding could results in different textures (e.g. Sundberg and Cooper, 2008). In our sample a combination of several processes may be responsible of the texture. However, due to the low volume fraction of the orthopyroxene, we should be cautious about any inferences. Some correlation could be established with the orthopyroxene texture in sample A6 (Zhao, 1997), a porphyroclastic mylonite from Morin Shear Zone.

7.2. Velocities of phases an composite

For single crystal P-waves, andesine is most anisotropic ($AV_P = 44.1\%$; $V_{Pmax} = 7.92$ km/s, $V_{Pmin} = 5.89$ km/s), clinopyroxene is intermediate ($AV_P = 39.8\%$; $V_{Pmax} = 9.35$ km/s, $V_{Pmin} = 7.16$ km/s), and orthopyroxene is least anisotropic ($AV_P = 23.2\%$; $V_{Pmax} = 8.62$ km/s, $V_{Pmin} = 7.38$ km/s). The strongest shear wave splitting (dV_S) is shown by single crystal plagioclase, with a maximum of 1855 m/s about 45° to Z' (Fig. 6).

Seismic velocities for individual phases of the textured Morin mylonitic anorthosite are calculated from the polycrystal elastic tensor of each phase (Geometric mean, GM; Table 1B. In plagioclase and clinopyroxene the distribution of P-wave velocity is asymmetric with respect to sample axes *XYZ*, while for orthopyroxene the pattern is more symmetric (Fig. 8). In general V_{Pmax} is at a high angle to the foliation (75°–90°) and V_{Pmin} defines an inclined girdle (≈15°) for plagioclase and a relatively wide maximum around the lineation in both pyroxenes (Fig. 8). Shear-wave splitting shows a complex pattern with no simple relationship with the foliation and lineation (Fig. 8). Both the shear-wave splitting and the orientation of the polarization plane for the fastest shear wave (S_1) are strongly dependent of the propagation direction.

In polyphase anorthosite seismic velocity (Fig. 7) is similar to the monomineralic aggregates, particularly to the plagioclase velocity patterns (100% Pl; Fig. 8). While plagioclase dominates the aggregate (88%), the contribution of pyroxenes (12%) to the bulk velocity is significant (Figs. 7 and 8). Comparing P-wave maximum velocity the mylonitic anorthosite shows higher values (7.10 km/s; Fig. 7) than pure plagioclase aggregate (6.71 km/s; Fig. 8). Real anisotropy also increases from $AV_P = 2.26\%$ to $AV_P = 2.36\%$.

We compared our elasticity data with those measured and calculated in similar samples by Ji et al. (1997), Zhao (1997) and Xie et al. (2003). P-wave velocities are similar, but with some differences due to compositional variations and averaging schemes (Table 2). Considering Voigt and Geometric Mean averages, actual anisotropy in our sample ($AV_P = 2.57–2.36\%$) is lower than calculated values of Xie et al. (2003) (3.33%), and Ji et al. (1997) (2.9%). The difference is larger compared to experiments by Zhao (1997) in terms of anisotropy ($AV_P = 4.2–8.5\%$) and shear-wave splitting (Table 2). In the aggregates from Xie et al. (2003) and Ji et al. (1997) a random pyroxene orientation was assumed. In Zhao (1997) a real texture for pyroxene was obtained for two samples, and then imposed on the rest of samples. Here the method to analyze the texture and the overall composition play an important role to

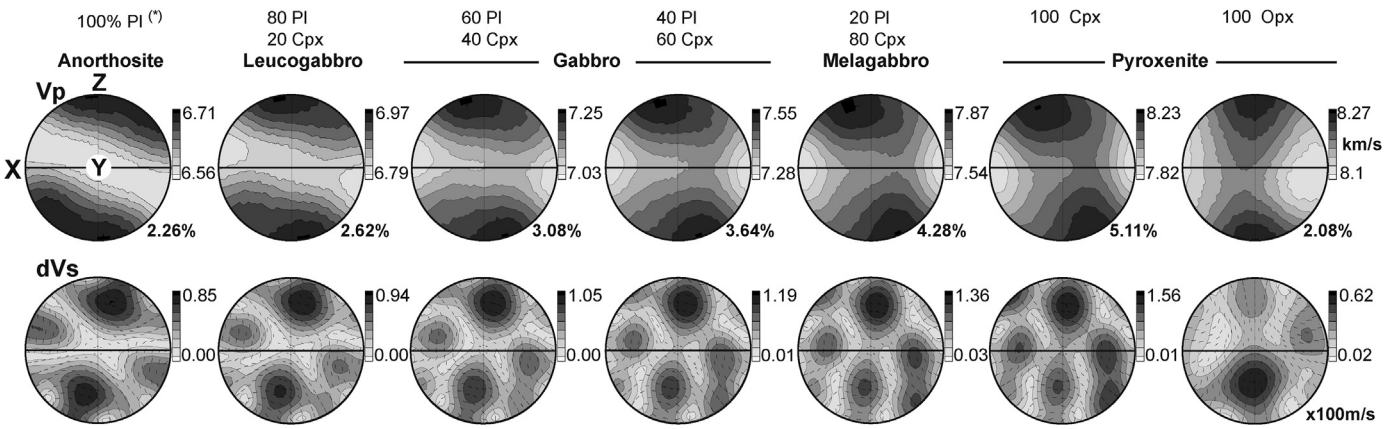

Fig. 8. P-wave velocity (V_P) and S-wave splitting (dVs) propagation surfaces (Voigt mean) for hypothetical combinations of plagioclase and clinopyroxene. Actual P-wave anisotropy (AVp, %) is indicated. Only significant mixtures for mafic mylonites are shown. Pure orthopyroxene aggregate are included for comparison. Same reference system *XYZ* as in Fig. 7. (*) Pl: plagioclase, Cpx: clinopyroxene, Opx: orthopyroxene.

explain those differences. For example, the U-stage measurements typically result in poor grain statistics and, in the case of plagioclase, a biased orientation/grain selection (e.g. Ji et al., 1994). Therefore some texture components could be artificially enhanced or removed. This is relevant, since both plagioclase and pyroxene fabrics could result in constructive or destructive combinations of their seismic behavior, depending on texture. The effect of the composition will be discussed later.

We can compare seismic data and ultrasonic measurements from previous studies (Ji et al., 1997; Zhao, 1997; $V_{P\ mean}$ = 6.9–6.5 km/s; Table 2) with those calculated along the sample coordinates (*X*, *Y*, *Z*; Fig. 1). Results with the same averaging scheme (Voigt) are similar ($V_{P\ mean}$ = 7.0 km/s), but even better for the Geometric Mean data ($V_{P\ mean}$ = 6.8 km/s). P-wave anisotropy depicts the same trend, with real data that range between AV_{Px-z} = 1.7–1.2% (Ji et al., 1997; Zhao, 1997), and our V_{Pxyz} data between AV_{Px-z} = 2.1 and 1.9% (Voigt–Geo Mean). It is clear that the difference between actual anisotropy and *XYZ* anisotropy (orientation of the cores for ultrasonic measurements in the sample reference system) is due to the effect of texture (e.g. Wenk et al., 2012). The selection of the averaging scheme (Voigt, Reuss, Hill, Geometric Mean) has some effect. In our case the best approximation to real velocity measurements is obtained with the Geometric mean.

7.3. Rock recipes. Anisotropy of gabbroic rocks

As a next step we are creating hypothetical plagioclase–clinopyroxene mixtures ('rock recipes'; Tatham et al., 2008), assuming that the phases display the same texture patterns The results are summarized in Tables 2 and 3 and Figs. 8–11. Orthopyroxene is not considered in the synthetic mixtures.

Elastic tensors for some relevant metagabbroic compositions are shown in Table 1C, and wave surfaces are displayed in Fig. 8. Both velocity and anisotropy increase with the pyroxene volume fraction from 6.7 to 8.3 km/s and from 2.3 to 5.1% respectively (Fig. 9). The trend of S-wave splitting is somewhat more complex but also increases (from 850 m/s to 1560 m/s; Figs. 8 and 9). The effect of texture in seismic properties is also clear in the synthetic mixtures. In Fig. 10, the variation of P-waves at different orientations to the lineation (*X*-axis), in the *XZ* sample plane reveal an asymmetric distribution around the foliation pole (75–80° to the *Z*-axis, Figs. 8 and 10), which could result in discrepancies between ultrasonic and texture-based seismic wave data. The dimension of that discrepancy is computed in terms of anisotropy in Fig. 11 (see also Table 3), where AV_{Px-z} and AV_P anisotropies are plotted against the bulk density of the plagioclase–pyroxene mixture (Pl-Cpx). A deviation of up to 25% from the actual value of P-wave anisotropy is expected if ultrasonic measurements are performed along the

Table 3
Texture-based seismic velocity models were calculated for synthetic mylonitic mixtures of plagioclase and clinopyroxene (Pl-Cpx). We used texture data from this study, and several combinations to calculate densities, P-waves velocities, S-wave splitting, and actual anisotropy (AV_P, %). Velocities along sample coordinates (Fig. 1) and derived anisotropy are also presented ($AV_{P(xz)}$, %). *V*: Voigt average; GM: Geometric Mean average.

	Synthetic mixtures											
%Pl	100		80		60		40		20		0	
%Cpx	0		20		40		60		80		100	
Average	*V*	GM	*V*	GM	*V*	GM	*V*	GM	*V*	GM	*V*	GM
V_{Pmax} (km/s)	6.88	6.71	7.24	6.97	7.56	7.25	7.84	7.55	8.09	7.87	8.34	8.23
V_{pmin} (km/s)	6.72	6.56	7.03	6.79	7.28	7.03	7.51	7.28	7.71	7.54	7.90	7.82
dVsmax (m/s)	108	85	103	94	108	105	116	119	125	136	135	165
dVsmin (m/s)	0	0	2	0	2	0	3	1	1	3	3	1
AV_p (%)	2.35	2.26	2.94	2.62	3.77	3.08	4.30	3.64	4.81	4.28	5.42	5.11
V_{pX} (km/s)	6.76	6.59	7.04	6.81	7.29	7.04	7.51	7.28	7.71	7.54	7.91	7.82
V_{pY} (km/s)	6.72	6.56	7.07	6.82	7.39	7.09	7.66	7.39	7.91	7.70	8.15	8.04
V_{pZ} (km/s)	6.87	6.71	7.22	6.96	7.53	7.24	7.81	7.53	8.06	7.83	8.29	8.17
V_p mean	6.78	6.62	7.11	6.86	7.40	7.12	7.66	7.40	7.89	7.69	8.10	8.01
AV_p (*xz*)(%)	1.62	1.81	2.53	2.19	3.24	2.81	3.92	3.38	4.43	3.77	4.68	4.37
ρ (g/cm^3)	2.72		2.83		2.94		3.05		3.16		3.26	

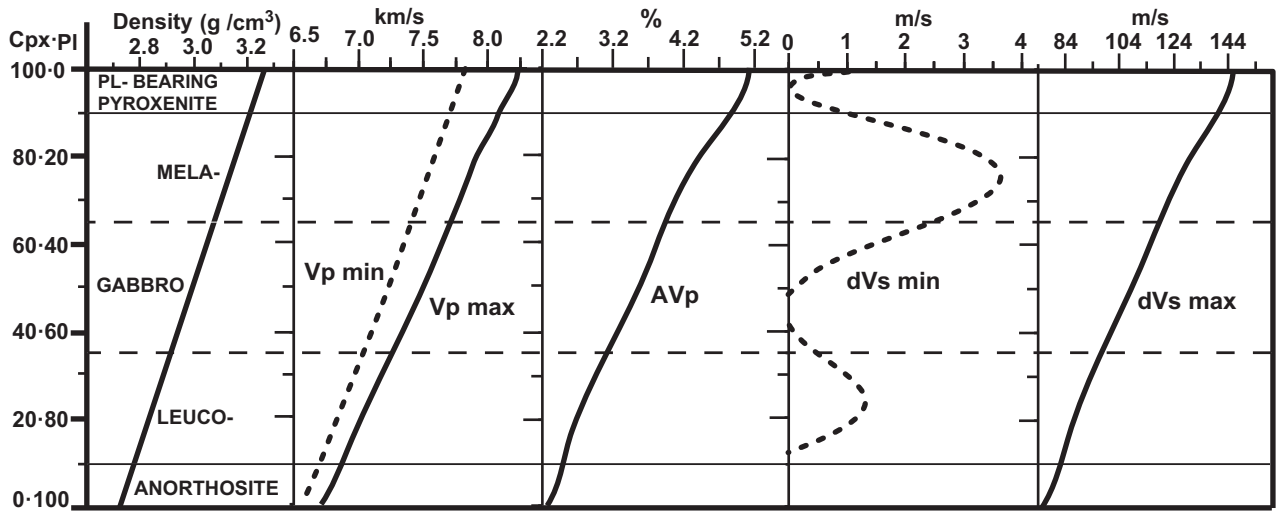

Fig. 9. Evolution of P- and S-wave velocities and anisotropy (AV_P) with composition (Cpx-Pl). Modal intervals for important rock types are based on Le Maitre et al. (2005).

Cartesian axes *X*, *Y*, *Z* (Fig. 11). This effect must be taken into account for the prediction and interpretation of seismic data, when monoclinic or triclinic texture symmetry is suspected (Fig. 5). The results highlight the need to expand the calibration of the seismic response to deformation fabrics for rocks at lower crust and different strain regimes (e.g. Lloyd et al., 2011).

7.4. Reflectivity

Reflection coefficients (R) at lithologic interfaces have been calculated from densities and P-waves velocities along the *Z*-axis (Geometric mean; Table 3; normal incidence, Sheriff and Geldart, 1995). Results calculated from synthetic mixtures and the mylonitic anorthosite (MSZ) are shown in Table 4. The pair mylonitic pyroxenite–anorthosite returns the highest reflectivity ($R = 0.035$). Among the gabbroic protoliths, mylonitic melagabbros have the highest contrast with mylonitic anorthosites ($R = 0.020$). Mylonites from gabbros and leucogabbros show a very low contrast with mylonitic anorthosites ($R < 0.011$).

Reflectivity results suggest that only when a strong mineral segregation occurs in mafic mylonites a good reflectivity could be reached between layers with pyroxene and layers with plagioclase ($R \approx 0.04$; Sheriff, 1975). Mechanical segregation of phases could be favored in high-grade shear zones affecting mafic protoliths because of the contrasting mechanical behavior of e.g. plagioclase and pyroxene (e.g. Mackwell et al., 1998).

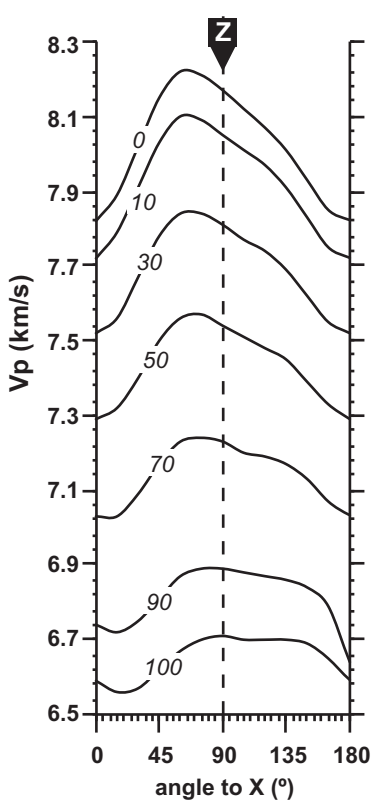

Fig. 10. Projection of P-wave velocity at different orientations to the sample lineation (*X*-axis) for different compositions (*XZ* plane). An asymmetric distribution is revealed. Each curve represents a distinct mixture of plagioclase and clinopyroxene (%Pl is indicated).

8. Conclusions

A sample from the Morin anorthosite shear zone was analyzed with TOF neutron diffraction. Texture and microstructures are compatible with the plastic deformation of the aggregate under high-T conditions. All mineral phases depict a significant preferred orientation that could be related to the general kinematic history of the Morin Shear Zone.

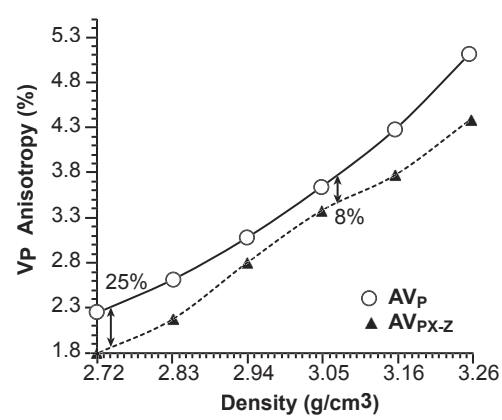

Fig. 11. P-wave anisotropy for different mixtures of plagioclase and clinopyroxene, here represented by their densities (see Table 2). Actual anisotropy (AV_P) based in true $V_{Pmax-min}$, and anisotropy (AV_{Px-z}) based on sample coordinates measurements (*XYZ*), returns different values. Difference in % is indicated.

Table 4
Reflection coefficients (R) at selected lithologic interfaces. Plagioclase–clinopyroxene synthetic mixtures are indicated by the Plagioclase fraction (%Pl). Mylonitic anorthosite from this study (MSZ). For the calculations we assume normal incidence. P-wave velocity along Z sample axis (V_{Pz}, Voigt mean) and corresponding densities (ρ (Tables 2 and 3) are used (Sheriff and Geldart, 1995).

	100Pl	70Pl	50Pl	30Pl	0Pl	MSZ
100Pl	0.000	0.004	0.011	0.020	0.035	0.000
70Pl			0.002	0.006	0.015	0.002
50Pl	$R = \frac{(V\rho_2 - V\rho_1)^2}{(V\rho_2 + V\rho_1)^2}$			0.001	0.007	0.007
30Pl					0.002	0.014
0Pl						0.027
MSZ						0.000

Texture-based elastic properties of the aggregate were calculated and compared with previous calculated and measured data in the area. A good agreement is found, but neutron diffraction, in combination with Rietveld data analysis emerges as a powerful technique to quantify preferred orientation of rocks composed of several low-symmetry phases.

We have explored the elastic properties of gabbroic rocks by using a 'rock recipes' approach. There is an increase of P-waves velocity, S-waves splitting and anisotropy for higher clinopyroxene volume fractions. Seismic anisotropy calculations are very sensitive to the texture symmetry. Large deviations (8–25%) were found between actual anisotropy (AV_P, V_{Pmax}, V_{Pmin}) and that measured along XYZ sample directions (AV_{Px-z}, V_{Px}, V_{Py}, V_{Pz}). This should be considered when interpreting geophysical data and building models of the lower crust, where textures with monoclinic and triclinic symmetries are common. Particularly preferred orientation patterns in more mafic gabbroic rocks should be analyzed with similar techniques.

Acknowledgments

The sample was collected on a fieldtrip organized by J. Martignole and S. Ji on occasion of ICOTOM 12 in Montreal. This contribution has been funded by the research project CGL2011-22728 of the Spanish Ministry of Science and Innovation, as part of the National Program of Projects in Fundamental Research, in the frame of the VI National Plan of Scientific Research, Development and Technologic Innovation 2008–2011. JGB appreciates financial support by the Spanish Ministry of Science and Innovation through the Ramón y Cajal program and funds from the Fulbright – José Castillejo program of the Spanish Ministry of Education, Culture and Sports (Programa Nacional de Movilidad de Recursos Humanos – Plan Nacional de I-D + i 2008–2011) (RYC-2010-05818 and CAS12/00156). Access to HIPPO – LANSCE is kindly appreciated. HRW acknowledges support from NSF (EAR-1343908-) and DOE (DE-FG02-05ER15637). We are grateful to Luiz F. G. Morales and Holger Stünitz for thorough and constructive reviews and to Dave Prior for the editorial work. We are appreciative of M. Sintubin for the invitation to participate in this volume to commemorate Henk Zwart, who inspired many of us.

References

Amiguet, E., Raterron, P., Cordier, P., 2010. Deformation of diopside single crystals at mantle pressure. TEM characterization of dislocation microstructures. Eur. J. Mineral. 22, 181–187.
Avé Lallemant, H., 1978. Experimental deformation of diopside and websterite. Tectonophysics 48, 1–27.
Bascou, J., Barruol, G., Vauchez, A., Mainprice, D., Egydio-Silva, M., 2001. EBSD-measured lattice-preferred orientations and seismic properties of eclogites. Tectonophysics 342, 61–80.
Bascou, J., Tommasi, A., Mainprice, D., 2002. Plastic deformation and development of clinopyroxene lattice preferred orientations in eclogites. J. Struct. Geol. 24, 1357–1368.
Beaumont, C., Jamieson, R.A., Nguyen, M.H., Lee, B., 2001. Himalayan tectonics explained by extrusion of a low-viscosity crustal channel coupled to focused surface denudation. Nature 414, 738–742.
Brace, W.F., Kohlstedt, D.L., 1980. Limits on lithostatic stress imposed by laboratory experiments. J. Geophys. Res. 85, 6248–6252.
Brenker, F., Prior, D., Müller, W., 2002. Cation ordering in omphacite and effect on deformation mechanism and lattice preferred orientation LPO. J. Struct. Geol. 24, 1991–2005.
Brown, J.M., Abramson, E.H., Angel, R.J., 2006. Triclinic elastic constants for low albite. Phys. Chem. Mineral. 33, 256–265.
Buatier, M., Van Roermund, H., Drury, M., Lardeaux, J., 1991. Deformation and recrystallisation mechanisms in naturally deformed omphacites from the Sesia-Lanzo zone; geophysical consequences. Tectonophysics 195, 11–27.
Bürgmann, R., Dresen, G., 2008. Rheology of the lower crust and upper mantle: evidence from rock mechanics, geodesy, and field observations. Annu. Rev. Earth Planet. Sci. 36, 531–567.
Burov, E.B., Watts, A.B., 2006. The long-term strength of continental lithosphere: "jelly sandwich" or "crème brûlée"? GSA Today 12, 4–10.
Bystricky, M., Mackwell, S., 2001. Creep of dry clinopyroxene aggregates. J. Geophys. Res. 106 (B7), 13443–13454.
Chen, W.P., Molnar, P., 1983. Focal depths of intracontinental and intraplate earthquakes and their implications for the thermal and mechanical properties of the lithosphere. J. Geophys. Res. 88, 4183–4214.
Christensen, N.I., Lundquist, S.M., 1982. Pyroxene orientation within the upper mantle. Geol. Soc. Am. Bull. 93, 279–288.
Cook, F.A., Velden, A. van der, Hali, R., Roberts, B.R., 1997. Lithoprobe SNORCLE-ing beneath the Northwestern Canadian shield. Lithoprobe Res. Notes 10, 59–64.
Dimanov, A., Dresen, G., 2005. Rheology of synthetic anorthite-diopside aggregates: implications for ductile shear zones. J. Geophys. Res. 110, B07203.
Dimanov, A., Rybacki, E., Wirth, R., Dresen, G., 2007. Creep and strain-dependent microstructures of synthetic anorthite-diopside aggregates. J. Struct. Geol. 29, 1049–1069.
Doig, R., 1991. U-Pb Zircon dates of the Morin anorthosite suite rocks, Grenville Province, Québec. J. Geol. 99, 729–738.
Dornbusch, H.J., Weber, K., Skrotzki, W., 1994. Development of microstructure and texture in high-temperature mylonites from the Ivrea Zone. In: Bunge, H.J., Siegesmund, S., Skrotzki, W., Weber, K. (Eds.), Textures of Geological Materials. DGM Informationsgesellschaft, Oberursel, pp. 187–201.
Ellis, S., Stöckhert, B., 2004. Imposed strain localization in the lower crust on seismic timescales. Earth Planets Space 56, 1103–1109.
Feinberg, J., Wenk, H.-R., Scott, G.R., Renne, P., 2006. Preferred orientation and anisotropy of seismic and magnetic properties in gabbronorites from the Bushveld layered intrusion. Tectonophysics 420, 345–356.
Fitz Gerald, J.D., Parise, J.B., Mackinnon, I.D.R., 1986. Average structure of an An48 plagioclase from the Hogarth Ranges. Am. Mineral. 71, 1399–1408.
Franke, W., 1995. Exhumation of Saxonian granulites: geological, petrological and isotopic constraints. Terra Nostra 95, 22–24.
Gatta, G.D., Rinaldi, R., Knight, K.S., Molin, G., Artioli, G., 2007. High temperature structural and thermoelastic behaviour of mantle orthopyroxene: an in situ neutron powder diffraction study. Phys. Chem. Mineral. 34, 185–200.
Godard, G., Van Roermund, L., 1995. Deformation-induced clinopyroxenes fabrics from eclogites. J. Struct. Geol. 17, 1425–1443.
Gómez Barreiro, J., Lonardelli, I., Wenk, H.R., Dresen, G., Rybacki, E., Ren, Y., Tomé, C.N., 2007. Orientation of anorthite deformed experimentally in Newtonian creep. Earth Planet. Sci. Lett. 264, 188–207.
Gómez Barreiro, J., Martínez Catalán, J.R., Prior, D., Wenk, H.-R., Vogel, S., Díaz García, F., Arenas, R., Sánchez Martínez, S., Lonardelli, I., 2010. Fabric development in a middle Devonian Intraoceanic Subduction regime: the Careón Ophiolite (Northwest Spain). J. Geol. 118, 163–186.
Gómez Barreiro, J., Martínez Catalán, J.R., 2012. The Bazar shear zone (NW Spain): microstructural and Time-of-Flight neutron diffraction analysis. J. Virtual Explor. 41 (paper 5).
Hill, R., 1952. The elastic behavior of a crystalline aggregate. Proc. Phys. Soc. A65, 349–354.
Homburg, J.M., Hirth, G., Kelemen, P.B., 2010. Investigation of the strength contrast at the Moho: a case study from the Oman Ophiolite. Geology 38, 679–682.
Indares, A., Martignole, J., 1990. Metamorphic constraints on the tectonic evolution of the allochthonous monocyclic belt of the Grenville Province, western Quebec. Can. J. Earth Sci. 27, 371–386.
Ingrin, J., Doukhan, N., Doukhan, J., 1991. High-temperature deformation of diopside single crystal-2. Transmission electron microscopy investigation of the defect microstructures. J. Geophys. Res. 96 (B9), 14287–14297.
Jackson, J., 2002. Strength of the continental lithosphere: time to abandon the jelly sandwich? GSA Today 12, 4–9.
Jackson, J.M., Sinogeikin, S.V., Bass, Jay D., 2007. Sound velocities and single-crystal elasticity of orthoenstatite to 1073K at ambient pressure. Phys. Earth Planet. Interior. 161, 1–12.
Ji, S., Mainprice, D., Boudier, F., 1988. Sense of shear in high temperature movement zones from the fabric asymmetry of plagioclase feldspars. J. Struct. Geol. 10, 73–81.
Ji, S., Mainpraice, D., 1988. Natural deformation fabrics of plagioclase: implications for slip systems and seismic anisotropy. Tectonophysics 147, 145–163.
Ji, S., Mainprice, D., 1990. Recrystallization and fabric development in plagioclase. J. Geol. 98, 65–79.
Ji, S., Salisbury, M., 1993. Shear-wave velocities, anisotropy and splitting in high grade mylonites. Tectonophysics 221, 453–473.

Ji, S., Zhao, X., Zhao, P., 1994. On the measurement of plagioclase lattice preferred orientations. J. Struct. Geol. 16, 1711–1718.
Ji, S., Long, C., Martignole, J., Salisbury, M., 1997. Seismic reflectivity of a finely layered, granulite–facies ductile shear zone in the southern Grenville Province (Quebec). Tectonophysics 279, 113–133.
Ji, S., Jiang, Z., Rybacki, E., Wirth, R., Prior, D., Xia, B., 2004a. Strain softening and microstructural evolution of anorthite aggregates and quartz–anorthite layered composites deformed in torsion. Earth Planet. Sci. Lett. 222, 377–390.
Ji, S., Wang, Q., Xia, B., 2004b. Mechanical properties of multiphase materials and rocks: a simple phenomenological approach using generalized means. J. Struct. Geol. 24, 1377–1390.
Kaercher, P.M., Militzer, B., Wenk, H.R., 2014. Ab initio calculations of elastic constants of plagioclase feldspars. Am. Mineral. http://dx.doi.org/10.2138/am.2014.4796.
Kanagawa, K., Shimano, H., Hiroi, Y., 2008. Mylonitic deformation of gabbro in the lower crust: a case study from the Pankenushi gabbro in the Hidaka metamorphic belt of central Hokkaido, Japan. J. Struct. Geol. 30, 1150–1166.
Kocks, U.F., Tomé, C.N., Wenk, H.R. (Eds.), 2000. Texture and Anisotropy—Preferred Orientations in Polycrystals and their Effects on Materials Properties. Cambridge University Press, Cambridge.
Kohlstedt, D.L., Evans, B., Mackwell, S.J., 1995. Strength of the lithosphere: constraints imposed by laboratory experiments. J. Geophys. Res. 100, 17587–17602.
Kruhl, J.H., 1987. Preferred lattice orientations of plagioclase from amphibolite and greenschist facies rocks near the Insubric Line (Western Alps). Tectonophysics 135, 233–242.
Kruse, R., Stünitz, H., Kunze, K., 2001. Dynamic recrystallization processes in plagioclase porphyroclasts. J. Struct. Geol. 23, 1781–1802.
Kruse, R., Stünitz, H., Kunze, K., 2002. Erratum to "Dynamic recrystallization processes in plagioclase porphyroclasts": [Journal of Structural Geology 23 (2001) 1781–1802]. J. Struct. Geol. 24, 587–589.
Le Maitre, R.W., Streckeisen, A., Zanettin, Le Bas, Bonin, B., Bateman, P., 2005. Igneous Rocks: a Classification and Glossary of Terms. Recommendations of the International Union of Geological Sciences Subcommission on the Systematics of Igneous Rocks. Cambridge University Press.
Lloyd, G.E., Butler, R.W.H., Casey, M., Tatham, D.J., Mainprice, D., 2011. Constraints on the seismic properties of the middle and lower continental crust. In: Geological Society of London Special Publications, vol. 360, pp. 7–32.
Lutterotti, L., Matthies, S., Wenk, H.-R., Schultz, A.J., Richardson, J.W., 1997. Combined texture and structure analysis of deformed limestone from time-of-flight neutron diffraction spectra. J. Appl. Phys. 81, 594–600.
Mackwell, S.J., Zimmerman, B.E., Kohlstedt, D.L., 1998. High temperature deformation of dry diabase with application to tectonics on Venus. J. Geophys. Res. 103, 975–984.
Maggi, A., Jackson, J.A., McKenzie, D., Priestley, K., 2000. Earthquake focal depths, effective elastic thickness, and the strength of the continental lithosphere. Geology 28, 495–498.
Martignole, J., Friedman, R., 1998. Geochronological constraints on the last stages of terrane assembly in the central part of the Grenville Province. Precamb. Res. 92, 145–162.
Matthies, S., Humbert, M., 1995. On the principle of a geometric mean of even-rank symmetric tensors for textured polycrystals. J. Appl. Crystallogr. 28, 254–266.
Matthies, S., Wenk, H.-R., 2009. Transformations for monoclinic crystal symmetry in texture analysis. J. Appl. Crystallogr. 42, 564–571.
McLelland, J.M., Selleck, B.W., Bickford, M.E., 2010. Review of the Proterozoic evolution of the Grenville Province, its Adirondack outlier, and the Mesoproterozoic inliers of the Appalachians. In: Tollo, R.P., Bartholomew, M.J., Hibbard, J.P., Karabinos, P.M. (Eds.), From Rodinia to Pangea: the Lithotectonic Record of the Appalachian Region, Geological Society of America Memoir, vol. 206, pp. 21–49.
Mehl, L., Hirth, G., 2008. Plagioclase preferred orientation in layered mylonites: evaluation of flow laws for the lower crust. J. Geophys. Res. 113, B05202.
Ranalli, G., 2003. How soft is the crust? Tectonophysics 361, 319–320.
Ranalli, G., 1995. Rheology of the Earth. Chapman & Hall, London, 413 pp.
Raterron, P., Doukhan, N., Jaoul, O., Doukhan, J., 1994. High temperature deformation of diopside IV: predominance of 110 glide above 1000 °C. Phys. Earth Planet. Inter. 82, 209–222.
Rey, P., 1995. Seismic and tectono-metamorphic characters of the lower crust in Phanerozoic Areas. Tectonics 12, 580–590.
Rivers, T., Martignole, J., Gower, C.F., Davidson, A., 1989. New tectonic divisions of the Grenville Province. Tectonics 8, 63–84.
Ross, J.V., Nielsen, K.C., 1978. High-temperature flow of wet polycrystalline enstatite. Tectonophysics 44, 233–261.
Royden, L.H., Burchfiel, B.C., King, R.W., Chen, Z., Shen, F., Liu, Y., 1997. Surface deformation and lower crust flow in eastern Tibet. Science 276, 788–790.
Rutter, E.H., Brodie, K.H., 1992. Rheology of the lower crust. In: Fountain, D., Arculus, R., Kay, R. (Eds.), Continental Lower Crust. Elsevier, New York, pp. 201–267.
Rybacki, E., Dresen, G., 2000. Dislocation and diffusion creep of synthetic anorthite aggregates. J. Geophys. Res. 105, 26,017–26,036.
Sang, L., Vanpeteghem, C.B., Sinogeikin, S.V., Bass, J.D., 2011. The elastic properties of diopside, CaMgSi2O6. Am. Mineral. 96, 224–227.
Seront, B., Mainprice, D., Christensen, N.I., 1992. A determination of the 3-dimensional seismic properties of an anorthosite. Comparison between values calculated from petrofabric and direct laboratory measurements. J. Geophys. Res. 98, 2209–2221.
Sheriff, R.E., 1975. Factors affecting seismic amplitudes. Geophys. Prospect. 23, 125–138.
Sheriff, R.E., Geldart, L.P., 1995. Exploration Seismology. Cambridge University Press.
Skrotzki, W., 1994. Defect structure and deformation mechanisms in naturally deformed augite and enstatite. Tectonophysics 229, 43–68.
Sundberg, M., Cooper, R.F., 2008. Crystallographic preferred orientation produced by diffusional creep of harzburgite: effects of chemical interactions among phases during plastic flow. J. Geophys. Res. 113 (B12208), 1–16.
Tatham, J., Lloyd, G.E., Butler, R.W.H., Casey, M., 2008. Amphibole and lower crustal seismic properties. Earth Planet. Sci. Lett. 267, 118–128.
Tribaudino, M., Nestola, F., Meneghini, C., 2005. Rietveld refinement of clinopyroxenes with intermediate Ca-content along the join diopside-enstatite. Can. Mineral. 43, 1411–1421.
Tullis, J., 1990. Experimental studies of deformation mechanisms and microstructures in quartzo-feldspathic rocks. In: Barber, D.J., Meredith, P.G. (Eds.), Deformation Processes in Minerals, Ceramics and Rocks. Unwin Hyman, London, pp. 190–227.
Ullemeyer, K., Spalthoff, P., Heinitz, J., Isakov, N.N., Nikitin, A.N., Weber, K., 1998. The SKAT texture diffractometer at the pulsed reactor IBR-2 at Dubna: experimental layout and first measurements. Nucl. Instr. Methods A 412, 80–88.
Van Roermund, H., 1983. Petrofabrics and microstructures of omphacites in a high temperature eclogite from the Swedish Caledonides. Bull. Minéral. 106, 709–713.
Van Roermund, H., Boland, J., 1981. The dislocation substructures of naturally deformed omphacites. Tectonophysics 78, 403–418.
Wenk, H.R., Matthies, S., Donovan, J., Chateigner, D., 1998. BEARTEX: a Windows-based program system for quantitative texture analysis. J. Appl. Crystallogr. 31, 269–362.
Wenk, H.-R., Lutterotti, L., Vogel, S., 2003. Texture analysis with the new HIPPO TOF diffractometer. Nucl. Instrum. Methods A515, 575–588.
Wenk, H.-R., Lutterotti, L., Vogel, S.C., 2010. Rietveld texture analysis from TOF neutron diffraction data. Powder Diffr. 25, 283–296.
Wenk, H.-R., Vasin, R.N., Kern, H., Matthies, S., Vogel, S.C., Ivankina, T.I., 2012. Revisiting elastic anisotropy of biotite gneiss from the Outokumpu scientific drill hole based on new texture measurements and texture-based velocity calculations. Tectonophysics 570–571, 123–134.
Wodicka, N., Ketchum, J., Jamieson, R., 2000. Grenville metamorphism of monocyclic rocks. Can. Mineral. 38, 471–510.
Wong, I.G., Chapman, D.S., 1990. Deep intraplate earthquakes in the western United States and their relationship to lithospheric temperatures. Seismol. Soc. Am. Bull. 80, 589–599.
Xie, Y., Wenk, H.-R., Matthies, S., 2003. Plagioclase preferred orientation by TOF neutron diffraction and SEM-EBSD. Tectonophysics 370, 269–286.
Zhao, X.-O., 1997. Microstructure et petrofabrique des minéraux haute température: example du terrain du Morin, Province de Grenville, Québec. Université de Montréal, Canada. Ph.D. thesis.
Zhao, X., Ji, S., Martignole, J., 1997. Quartz microstructures and c-axis preferred orientations in high-grade gneisses and mylonites around the Morin anorthosite (Grenville Province). Can. J. Earth Sci. 34, 819–832.